



Discussion

Simple air-gap fiber Fabry–Perot interferometers based on a fiber endface with Sn-microsphere overlay

Cheng-Ling Lee*, Cheng-Hung Hung, Chai-Ming Li, Yan-Wun You

Department of Electro-Optical Engineering, National United University, Miaoli 360, Taiwan

ARTICLE INFO

Article history:

Received 23 April 2012

Received in revised form

25 June 2012

Accepted 26 June 2012

Available online 13 July 2012

Keywords:

Air-gap fiber Fabry–Perot interferometer (AG-PPFI)

Fiber optics component

Fiber sensor

Interference

ABSTRACT

This study presents a simple, cost-effective and sensitive air-gap fiber Fabry–Perot interferometer (AG-PPFI) which is based on a metal Tin (Sn)-overlaying fiber technique. An extremely small drop of metallic Sn was heated and then melted to shrink into a microsphere owing to the cohesion of the material. When a fiber was inserted into the melting Sn microsphere, an air gap was naturally formed between the fiber endface and the metal Sn during the cooling process. By carefully controlling the reaction time, various air-gaps can be formed as the Fabry–Perot interferometric cavities for the proposed AG-PPFIs. Measurements reveal that a smaller length of air-gap and heavier mass of Sn-microsphere are associated with higher sensitivity of temperature, but the former is dominated. A best temperature sensitivity of wavelength shift with $+4.3 \text{ nm}/^\circ\text{C}$ is achieved when the air-gap is about $5 \mu\text{m}$ with mass of Sn-microsphere of about $10 \mu\text{g}$. The variation of the wavelength shift is equivalent to sensitivity for a change in the cavity length of $+14.83 \text{ nm}/^\circ\text{C}$.

© 2012 Elsevier B.V. All rights reserved.

1. Introduction

Varieties of air gap fiber Fabry–Perot interferometers (AG-FFPI) have been proposed with many smart and hybrid structures to manage the wide fields of practical applications. These AG-FFPI devices especially based on all-fiber or integrated configurations are useful since they have simple, cost-effective, convenient and sensitive characteristics [1–13]. A simplest method for the AG-FFPI is used two aligned fiber endface which utilizes two reflections of optical light reflected by the first and second fiber/air interfaces to generate low-finesse interference fringes [1–3]. In [2], especially an extrinsic Fabry–Perot interferometer based on the alignment of sapphire fibers endface has been presented for high temperature multipoint sensing with high sensitivity. Some smart AG-FFPIs integrated as all-fiber configurations have been adapted to effectively sense surrounding parameters [4–13]. An intrinsic low-finesse Fabry–Perot smart configuration has been proposed by Kim et al. The air gap inside the AG-FFPI device was formed by hydrofluoric acid etching fiber endface and then by fusion process [4]. The all-fiber and intrinsic structure is useful and convenient for practical sensing. Thus, similar compact and intrinsic AG-FFPIs by using etching and splicing processes to form the air-gap of a certain distance as a Fabry–Perot cavity have also

been presented in [5]. Besides, a new technique involves use of fs-laser micromachining to carve the fiber to form the air-gap. This method is advanced, convenient and requires no alignment, but it does require an expansive laser [6,7]. Some AG-FFPIs formed with hybrid structures by using the special fusion techniques of different kinds of fibers have been reported and applied for many sensing applications [8,9]. Other smart configurations of AG-PPFIs, such as splicing an air bubble skillfully between the fiber and a photonic crystal fiber (PCF) [10] and splicing a section of a hollow core fiber (HCF) [11], are reportedly effective in the fabrication of the air-gap Fabry–Perot cavities. Recently, an ultracompact and sensitive AG-FFPI based on an UV-cured polymer filling hollow core fiber (HCF) endface has been presented [12]. The variation of the Fabry–Perot cavity length can be greatly enhanced from exploiting the high thermal expansion coefficient of the elastic polymer-filled in the HCF [12]. We also have presented a hybrid structure of a reflection long-period fiber grating (RLPFG) connected with an AG-FFPI for simultaneously sensing refractive index and temperature [13]. The air gap formed in the present AG-FFPI was formed by overlaying the endface of a fiber metallic tin (Sn) microsphere around. However, the optical characteristics of the proposed AG-FFPIs with Sn-microsphere overlay are still indistinct. Even the devices with different air gaps and different sizes of Sn-microsphere as well as the precise air gap control of fabrication are not discussed so far. Therefore, in this paper, we further successively fabricate AG-FFPI devices with different lengths of air gap with overlaying various size of

* Corresponding author. Tel.: +886 37 381732; fax: +886 37 351575.
E-mail address: cherry@nuu.edu.tw (C.-L. Lee).

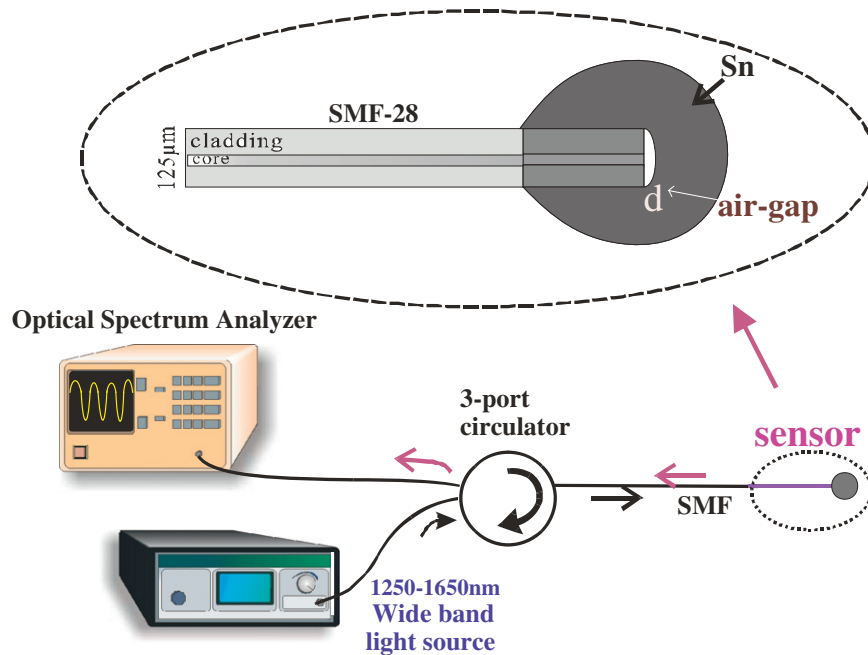


Fig. 1. Configuration of the proposed Sn-microsphere overlaying AG-FFPI.

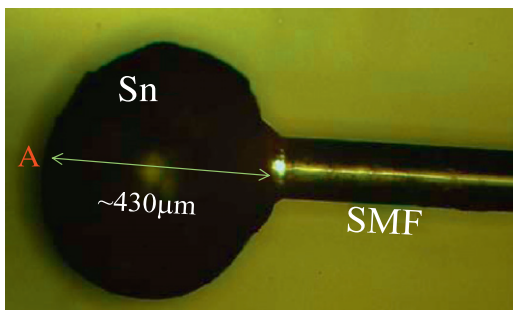


Fig. 2. Optical micrograph of the microsphere Sn-overlaying fiber endface.

Sn-microsphere and investigate the thermal expansion about the metal microsphere for sensing properties. Configuration of the proposed AG-FFPI with Sn microsphere overlaying is shown in Fig. 1. An SMF-28 fiber with a little amount of trapped air inserts into a melting Sn microsphere. When the Sn microsphere was cooling and became solid, an air gap with length of d is formed inside the sensor. The metal Sn used here can be easily processed because of its low melting point (231.9°C) and it is also a good electrical/thermal conductor. It is therefore extensively adopted in the electrical and electronics industries. Other metals for example aluminum (Al) or silver (Ag) also can be good candidates for much higher temperature sensing application.

The organization of this paper is as follows: in Section 2, the experiment for the proposed AG-FFPI with different structures has been presented. Section 3 contains the experimental results for comparison to those of the analyzed results in Section 2. Finally, the main conclusion has been drawn in Section 4.

2. Experimental

The air-gap cavity presented in this study is very simple and has high repeatability. Fabrication of the air-gap on the fiber endface is operated manually by hands with skillful experiences. When the fiber endface was inserted into an extremely small drop

of melting and shrunk Sn-microsphere, an air gap was formed which is shown in Fig. 2. By using the tip of a welding iron attaching an extremely small solid Sn metal, the Sn was melted and behaved like a sphere due to the surface tension. The welding iron was still attached at point A and not removed until the fiber insertion. Based on our experiences, by carefully controlling the insertion time of the fiber and cooling time of the melting Sn-microsphere, the air-gap length would be dominated substantially. Generally, faster insertion time would obtain a smaller air-gap during the Sn-microsphere is still melted. Now we can successfully fabricate the air-gap within the range around $5\text{--}37 \mu\text{m}$ by using the proposed method with the repeatability greater than 90% so far, as well as control the air-gap length with error of about $\pm 3 \mu\text{m}$ for different sizes of Sn-microsphere. One can see in Fig. 2, a bright spot is appeared in around middle of Sn-microsphere when light inputs the fiber. The light spot also can be anticipated as the location of the air gap inside the AG-FFPI sensor. The reason of the air inside the microsphere can be realized by a little air trapping through the adhesion process, an air-gap (void) is readily formed through the quick cooling process. We think it is the nature phenomenon of the adhesion process between the different kinds of material. Although the mechanical properties of the air-gap formed between the fiber and metal bulk have not been discussed in the published papers so far, a discussion about the adhesion process and air void formation in the interface of materials however can be found in [14]. Thus, we think that the void is probably not only at the interface between fiber end and Sn-metal, but also further existed on the side of the fiber due to the melting Sn which is not easy to spread coating on the fiber endface.

In measurement, the interference fringes of the AG-PPFIs with different structures are measured by an optical spectrum analyzer (OSA), and all displayed in Fig. 3. The interference mechanism in the proposed AG-FFPI is based on the low-finesse air-gap Fabry–Perot cavity since the reflections from the fiber/air and air/Sn interfaces are low, around 0.034 and 0.1–0.2 respectively. Because the Fabry–Perot air gap was formed between the surface of the Sn and the edge of the fiber, it can be estimated that high thermal expansion coefficient (TEC) of Sn with about $2.2 \times 10^{-5} \text{ }^\circ\text{C}^{-1}$

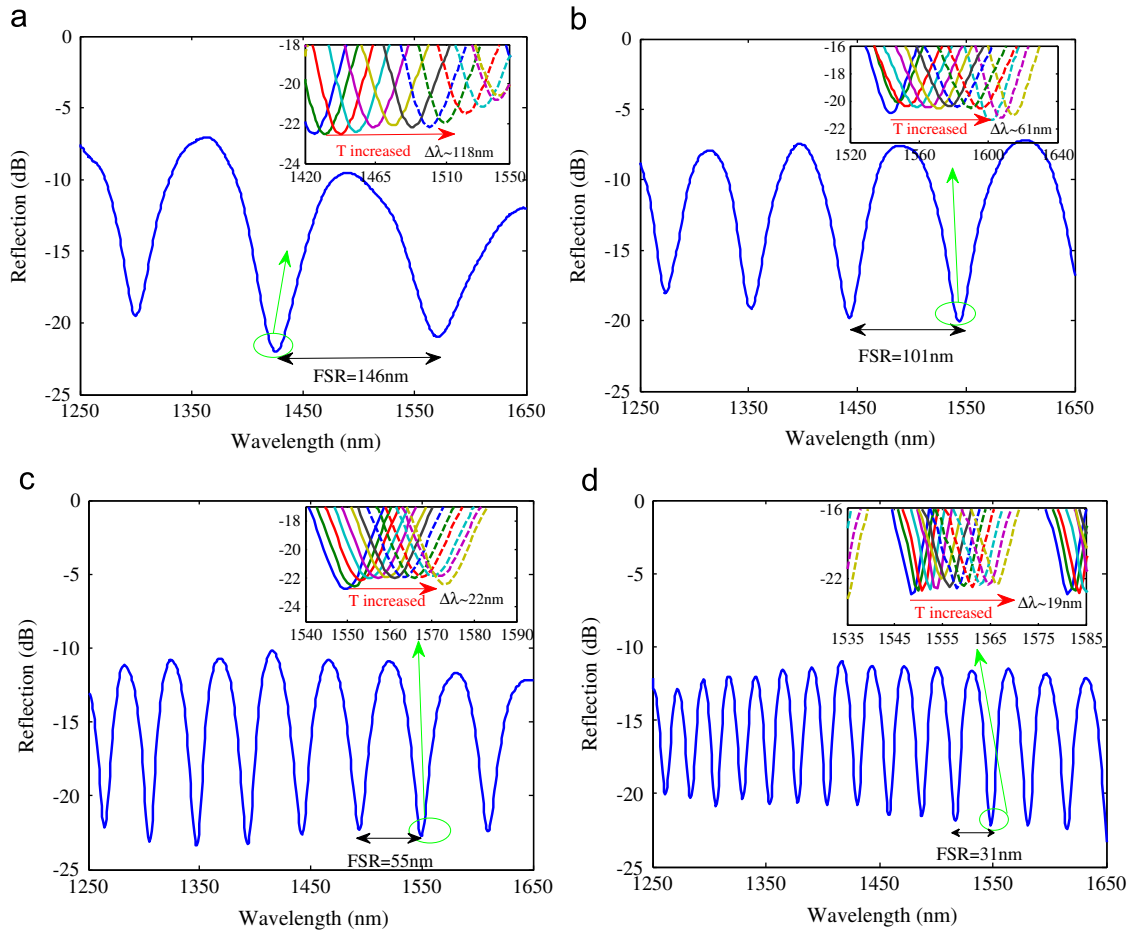


Fig. 3. Experimental reflection spectra of proposed devices with air-gap d of (a) 7 μm , (b) 11 μm , (c) 21 μm and (d) 37 μm with Sn mass of 3 μg . Inset respectively indicates the λ shift of interference dip when T increases from 25 $^{\circ}\text{C}$ to 85 $^{\circ}\text{C}$.

enables a high T sensitivity sensing. Fig. 3(a)–(d) shows the interference spectra of the various air-gaps of AG-FFPIs with mass of Sn as 3 μg at 25 $^{\circ}\text{C}$. Here d denotes the length of the air gap and the corresponding insets are respectively indicated by the wavelength shifts of T sensitivities for various d of AG-FFPI. The spectral interference fringes demonstrate that a longer cavity has a denser interference pattern and shorter free spectral range (FSR) over a given range of wavelengths. The overall insertion loss is about the range 7~12 dB for the devices even with different d . There are many factors that affect the insertion loss of the devices. For example, quality of the Sn-microsphere, fabricated skill and the length of air-gap. Experimental results of Fig. 3 also reveal that quasi-sinusoidal interference patterns over a very wide range of wavelengths in the cases of different air gap lengths.

3. Results and discussion

To demonstrate the effective sensing performance of T for the proposed AG-FFPI sensors with the different structures, sensors are placed on a TE cooler inside a closed space with the temperature T ($^{\circ}\text{C}$) increased from 25 $^{\circ}\text{C}$ to 85 $^{\circ}\text{C}$. The insets in Fig. 3(b)–(d) identically show the measured wavelength shift ($\Delta\lambda$) from spectral responses at wavelength dip around 1550 nm, which shift toward to the longer wavelength (λ) side as T increased. In Fig. 3(a) with the case of $d=7\ \mu\text{m}$, spectral interference dip about $\lambda=1450\ \text{nm}$ was monitored since the measured results of $\Delta\lambda$ from the dip around 1550 nm exceeds the measurement range when T increased from 25 $^{\circ}\text{C}$ to 85 $^{\circ}\text{C}$.

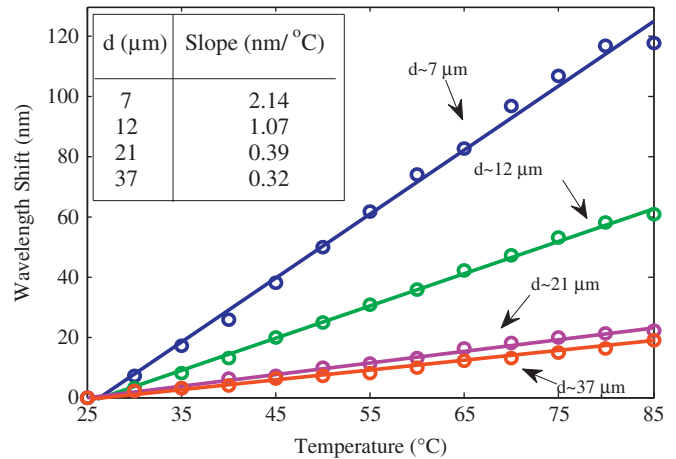


Fig. 4. Wavelength shifts of the spectral dips as a function of surrounding T in the air for various AG-FFPIs with Sn of 3 μg .

Fig. 4 plots T sensitivities of $\Delta\lambda$ for the AG-FFPIs with different lengths of air-gap based on the results of Fig. 3. The fitting curves display proportional relations between the wavelength shifts and temperature. Inset shows the sensitivity slope (S : $\text{nm}/^{\circ}\text{C}$) with 0.32~2.14 $\text{nm}/^{\circ}\text{C}$ for the d from 37 to 7 μm . Clearly, the S of the sensor caused by the thermal expansion effect of metal is much larger than those of the conventional long-period fiber gratings (LPG) based sensors (+0.04~0.1 $\text{nm}/^{\circ}\text{C}$). The experimental results also reveal that a smaller air-gap of Sn-microsphere is

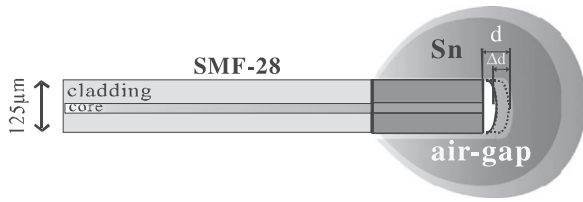


Fig. 5. Diagram for the variation of air gap (Δd) in the sensor by thermal expansion.

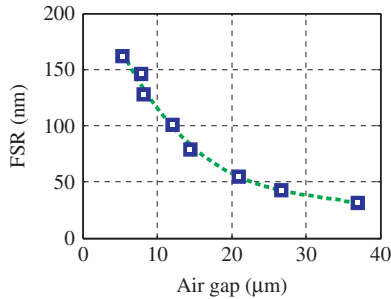


Fig. 6. Dependence of the FSR and the air-gap (d) for the AG-FFPIs.

associated with a higher sensitivity of temperature. Herein, the positive sensitivity of the proposed sensor means that the air gap increases due to the metal microsphere that was thermally expanded by the heating, shown as Fig. 5. It makes the wavelength dips red shifts. Force generated by the thermal expansion acts mainly on the side of the metal and changes the air-gap width (Δd) of the cavity, shown as. The Δd and wavelength shifts of the m th interference dip ($\Delta\lambda_m$) at the specific m th interference fringe (λ_m) satisfy the following relation:

$$\frac{\Delta d}{d} = \frac{\Delta\lambda_m}{\lambda_m} \quad (1)$$

Hence, one can see Eq. (1) a shorter d is more sensitive (i.e. $\Delta\lambda_m/\lambda_m$ is larger) and a poorer result is obtained as d increases. Besides, $\Delta\lambda_m$ is positive since the Δd increased by the linear thermal expansion of the metal. These results demonstrate the consistency of proportional relation in Fig. 4. From the experimental results of Fig. 3, the FSR of interference spectra are dominated by the length of air gap (d) of the Fabry–Perot cavity and the d can be estimated by the following form:

$$d = \frac{\lambda_1 \lambda_2}{2n \cdot \text{FSR}} \quad (2)$$

Here $n=1$ (air) in which λ_1 and λ_2 are the wavelengths corresponding to the subsequent minimum intensity of the reflection light (see Fig. 3), and FSR denotes $\Delta\lambda = \lambda_2 - \lambda_1$. Thus dependence of the FSR of the interference spectra and the air-gap (d) are plotted in Fig. 6.

However, there might be some other minor factors affecting the sensitivity of measurement, e.g. the amount of the air remained in the air-gap, and the mass of Sn microsphere attached in the sensor. The amount of the air cannot be estimated and minor effect to be ignored. Because the above results show that the temperature sensitivity (S) of the sensor is clearly dominated by the metal Sn microsphere. Therefore, different amounts of the metal-Sn around with almost the same air gap of the proposed AG-FFPIs are fabricated and tested in the study. Fig. 7 shows the S of the AG-PPFIs with different air gaps and various amounts of the Sn microsphere. From the results, a bigger Sn microsphere with Sn mass of $10 \mu\text{g}$ is a little more sensitive than that of smaller case of $3 \mu\text{g}$ and the best sensitivity are achieved with

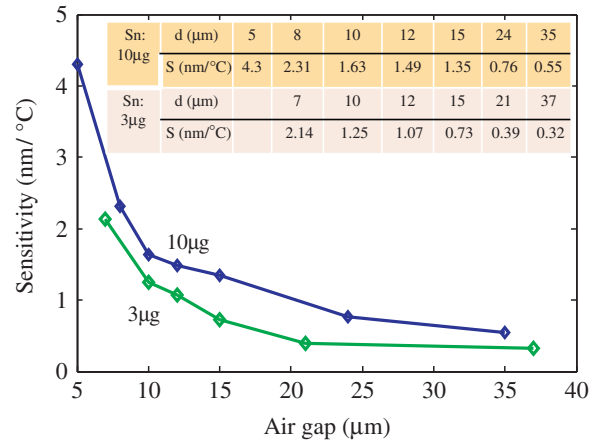


Fig. 7. Experimental results of the T sensitivities (S) of various AG-FFPIs with different d for the Sn mass of $3 \mu\text{g}$ and $10 \mu\text{g}$, respectively.

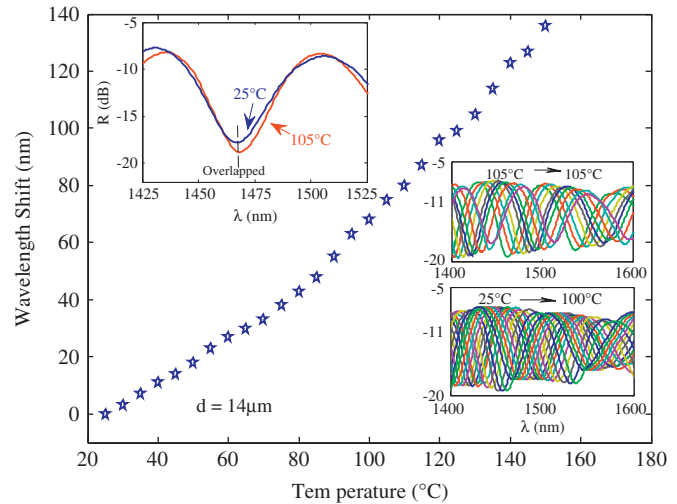


Fig. 8. Wavelength shifts of the spectral dips for high T sensing from $T=25 \sim 150 \text{ }^\circ\text{C}$ for the proposed AG-FFPI with $d \sim 14 \mu\text{m}$. Upper inset shows an overlap of dips occurred at $T=105 \text{ }^\circ\text{C}$ in this device.

temperature S approximately $4.3 \text{ nm}/^\circ\text{C}$ when the $d=5 \mu\text{m}$. Although the T sensitivity is much better than those of general fiber-based sensors, however, the measurement range is limited by the FSR of the interference fringes. An overlap of the wavelength dips may occur under a large T variation. The overlay causes an unidentified shift of the λ dips. Generally, shorter air-gaps would have greater T sensitivity but with smaller measurement range when considering the dips overlapped. An AG-FFPI with $d=14 \mu\text{m}$ has been tested for high T sensing to evaluate the maxima measurement range. The sensing results are shown in Fig. 8 below and also display a good linearity response in high T measurement. One can see that the overlap of the dips occurred around $T=105 \text{ }^\circ\text{C}$ which is the maxima measurement of T in the case of $d=14 \mu\text{m}$. Although the measurement range is not so high and would be the main drawback; however, the device presents a new and a simple structure for forming an air-gap Fabry–Perot interferometer with different gaps in the fiber tips. It may have more potential in some field of applications with these kinds of metal–fiber hybrid devices.

Another undesired property of the device would be the thermal hysteresis. Due to the nature of the metal expansion, the devices might have the hysteresis. To investigate the device about the thermal hysteresis property after a cycle of temperature

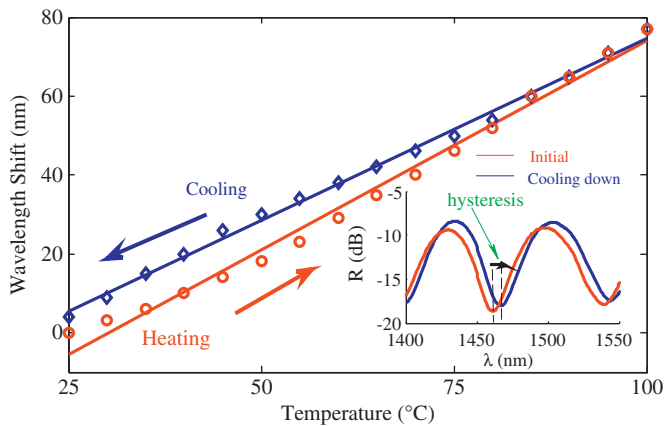


Fig. 9. Wavelength shifts of the spectral dips for heating and cooling processes of the proposed AG-FFPI with $d \sim 14 \mu\text{m}$. Inset shows the respective spectra of the initial (before heating) and cooling down after round trip of T treatment.

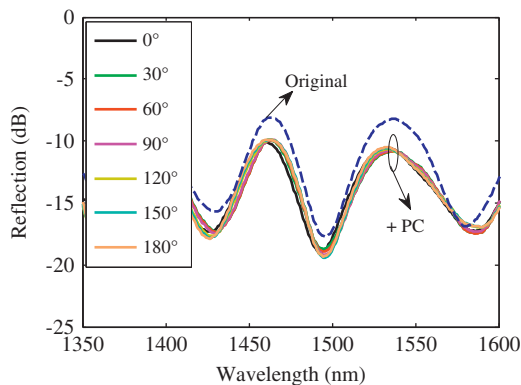


Fig. 10. Reflection spectra with different polarized states of incident light for the AG-FFPIs. An insertion loss about 2–3 dB is obtained when the device with the polarization controller (PC).

treatments, an AG-FFPI with d around $14 \mu\text{m}$ has been measured and the results are shown in Fig. 9. Fig. 9 shows that a spectral hysteresis with wavelength dips of $\Delta\lambda = 4 \text{ nm}$ corresponds to the thermal hysteresis of the air-gap around $\Delta d = (\Delta\lambda/\lambda) \cdot d = 38.6 \text{ nm}$ is generated after a cycle measurement. The hysteresis effect of air-gap is about $38.6 \text{ nm}/14 \mu\text{m} = 0.267\%$ in this case. Although the effect is small and under 1%, however the undesirable influence of this kind of metal (Sn)–fiber device is a drawback and would affect the measurement. Even so, there might be some other metals with lower thermal hysteresis which could be used as good candidates for reducing this effect.

Finally, to investigate the polarization dependence of this metal–fiber hybrid device, light propagates through a fiber polarization controller (PC) and inputs the device to observe the polarization sensitive of the sensors. In principle, light propagates into a flat boundary of air/metal with normal incidence

(i.e. incident angle $\theta = 0$), the reflection is polarization independent. However, due to the structure of the air-gap inside the Sn-microsphere of the device would be not very flat, thus the spectra still presents a very slight polarization dependence but not really distinct, as shown in Fig. 10. Fig. 10 shows the reflection spectra with a little variation of intensity by varying the polarized state of incident light. From the experimental results, the effect of polarization on the measurement of the proposed sensor is very little and can be ignored.

4. Conclusion

This work has demonstrated a simple, cost-effective and sensitive AG-FFPI with Sn microsphere overlaying on the fiber endface. Various air gaps can be formed between the surface of the metal Sn and the end of the fiber by using the proposed technique. The temperature sensitivity of the sensor is approximately several ten times greater than that of the conventional silica-based fiber gratings. The sensitivity of $+4.3 \text{ nm}/^\circ\text{C}$ is achieved when the air gap is about $5 \mu\text{m}$ with mass of Sn-microsphere $10 \mu\text{g}$, which is equivalent to sensitivity to a change in cavity length of $+14.83 \text{ nm}/^\circ\text{C}$. This device can provide the many advantages of simplicity, easy fabrication and high sensitivity for applying in a wide range of sensing systems.

Acknowledgment

This work was supported by the Research Project of the National Science Council of Taiwan, NSC 100-2221-E-239-038.

References

- [1] C.-L. Lee, W.-Y. Hong, H.-J. Hsieh, Z.-Y. Weng, IEEE Photonics Technology Letters 23 (23) (2011) 905.
- [2] J. Wang, B. Dong, E. Lally, J. Gong, M. Han, A. Wang, Optics Letters 35 (2010) 619.
- [3] D.-H. Kim, J.-W. Park, H.-K. Kang, C.-S. Hong, C.-G. Kim, Smart Materials and Structures 12 (2003) 1.
- [4] D.W. Kim, F. Shen, X. Chen, A. Wang, Optics Letters 30 (2005) 3000.
- [5] X. Chen, F. Shen, Z. Wang, Z. Huang, A. Wang, Applied Optics 45 (30) (2006) 7760.
- [6] T. Wei, Y. Han, Y. Li, H.-L. Tsai, H. Xiao, Optics Express 16 (8) (2008) 5764.
- [7] Y.-J. Rao, M. Deng, D.-W. Duan, X.-C. Yang, T. Zhu, G.-H. Cheng, Optics Express 15 (21) (2007) 14123.
- [8] Z. Huang, Y. Zhu, X. Chen, A. Wang, IEEE Photonics Technology Letters 17 (2005) 3403.
- [9] H.Y. Choi, K.S. Park, S.J. Park, U.-C. Paek, B.H. Lee, E.S. Choi, Optics Letters 33 (2008) 2455.
- [10] J. Villatoro, V. Finazzi, G. Coviello, V. Pruneri, Optics Letters 34 (16) (2009) 2441.
- [11] Y. Zhao, R.-Q. Lv, Y. Ying, Q. Wang, Optics and Laser Technology 44 (2012) 899.
- [12] C.L. Lee, L.H. Lee, H.E. Hwang, J.M. Hsu, IEEE Photonics Technology Letters 24 (2) (2012) 149.
- [13] C.L. Lee, W.F. Liu, Z.Y. Weng, F.C. Hu, IEEE Photonics Technology Letters 23 (2011) 1231.
- [14] M. Mukadam, J. Schake, P. Borgesen, K. Srihari, Thermal and Thermomechanical Phenomena in Electronic Systems 1 (2004) 58.